Continuous Long-Range Thunderstorm Monitoring by a VLF Receiver Network

Part I: Instrumentation and Location Error Analysis

Carlos A. Morales*

Department of Civil and Environmental Engineering, University of Connecticut, Storrs, CT 06269

James A. Weinman

Microwave Sensors Branch, NASA Goddard Space Flight Center, Greenbelt, MD 20771

Emmanouil N. Anagnostou

Department of Civil and Environmental Engineering, University of Connecticut, Storrs, CT 06269

J. Stanley Kriz

Resolution Displays Inc., Fairfax, VA 22301

*Current Affiliation: Atmospheric Sciences Department, Colorado State University, Fort Collins, CO

Corresponding author address: Dr. Carlos A. Morales, Atmospheric Sciences Dept, Colorado State University, CO 80523, E-mail: morales@atmos.colostate.edu

Submitted to *Journal of Atmospheric and Oceanic Technology*

January 2002

ABSTRACT

Lightning emits radio noise (sferics) over a broad region of the electromagnetic spectrum. Sferics in the Very Low Frequency (VLF) between 5 and 15 kHz propagate over thousands of kilometers in the earth-ionosphere wave-guide. An experimental network of five ground-based radio receivers, was situated along the US east coast and Puerto Rico. That network measured sferics between July 1997 and February 1998. In this study, sferics distributions from this experimental network are compared to lightning data form the US National Lightning Detector Network (NLDN) and the Lightning Imaging Sensor (LIS) onboard the TRMM satellite. An analysis which neglected non-linear propagation effects on pulse shapes produced location errors up to 100 kilometers due to uncertainties in signal processing, phase velocity modeling, and radio receivers' spatial configuration effects. After applying statistical corrections, North Atlantic Ocean and northwest South America regions location errors were reduced to less than 50 km. Expected errors derived from Monte Carlo simulation for this experimental network agreed with the errors retrieved from independent measurements with some moderate disagreement over the west coast of US. A location error correction scheme is developed, which combines theoretical and experimental models along with satellite infrared observations. Significant location error reduction is demonstrated, with corrected errors varying from less than 20 km to less than 60 km in the eastern and western part of US, respectively.

1. Introduction

Over the years infrared (IR) imagery from geo-stationary satellites has been practically the sole sensor for near-continuous global-scale cloud observations. Technology has recently advanced to the point where lightning can now be monitored continuously with reasonable cost over large regions by means of the radio noise that is emitted in the Very Low Frequency (VLF) range of 5 to 15 kHz. Those noise pulses, known as sferics, propagate over thousands of kilometers in the earth-ionosphere wave-guide, Budden(1951). Whereas IR imagery yields information on the height of cloud tops, lightning provides information about the interior structure of clouds.

Baker et al. (1995) have shown that charge separation in thunderstorms is produced by non-inductive ice-ice interactions at temperatures less than -10^{o}C and a critical range of super-cooled water concentrations. Updraft velocities within electrified precipitating clouds must be sufficiently intense to create an adequate differential velocity between dense, negatively charged, large ice particles and smaller, positively charged, snow particles. This charge separation gives rise to lightning discharges, which may take place between cloud and ground (CG) or, more frequently and earlier in the development of the thunderstorms, as intra-cloud (IC) lightning. Subsequently, lightning occurs in those regions of a cloud system associated with heavy precipitation, turbulence, and strong vertical velocities. Therefore, its determination by sferics measurements can be beneficial for numerous applications including weather forecasting, climatology, hydrology, and aviation operations.

Pierce (1977) described the physics of sferics based upon work conducted after World War II. In later years Lee (1986a, 1986b, 1988) developed a sferics observation network, which

currently provides operational lightning observations over much of Europe from receivers located in the UK, Gilbratar, and Cyprus. The work of the above authors has shown that such system can monitor lightning activities as far from Europe as Central America. Resolution Display Inc. (RDI) subsequently developed an experimental network of five ground receivers located along the US east coast and Puerto Rico. For convenience this sensor network is denoted as Sferics Timing and Ranging NETwork (STARNET). With the deployment of STARNET, sferics have been measured from central Brazil to northern Alberta and from the western US to the west coast of Europe.

Lightning location accuracy is valuable information for forthcoming applications of STARNET measurements. Lightning measurements have been extensively used by power plants and insurance companies, as well as by the meteorological and hydrological research community. It is noted that each of the above applications requires varying degree of location precision ranging from tens of meters up to tens of kilometers. Knowledge of the location error distribution is important for understanding the limitations of such measurements and further improving their accuracy through investigation of the various error sources. Expected location errors evaluated through Monte Carlo simulations are compared to relative location errors estimated by comparisons with other more established lightning networks over the continental US and Atlantic Ocean, Caribbean and South America. In the companion paper of Morales et al. (2002, this issue) we examine the system's efficiency in detecting cloud-to-ground and intra-cloud lightning. This paper will now describe the STARNET system and explore its lightning location errors.

2. Instrument System Overview

STARNET uses the general concept developed by Lee (1986b) on an operational Arrival Time Difference (ATD) system over Europe, however it benefited from Internet and (Global Positioning System (GPS) technology not available in the Lee's system. In the earlier version of Lee's network, the ATD system used atomic clocks for its time stamp and used phone lines to transmit the data that constrained the frequency of measurements to the stronger lightning strikes. The recent advances in Internet technology provides a wider bandwidth transmission that can provide higher data ingest rates compared to a few years ago. The experimental STARNET system presented herein is no longer operational. Nevertheless, an identical system with six receivers is currently being deployed in Europe and it is working experimentally since June of 2001.

The present network is based on radio sferics receivers in the VLF spectrum between 5 and 15 kHz centered at 9.8 kHz. Each receiver measures the vertical electric field and includes a time stamp synchronized to GPS clocks within one microsecond accuracy, where the sferics location is obtained by time differences in the impulsive noise emitted by a lightning strike. These electric field time series represent sferics waveforms of a lightning source that propagates through the ionosphere-earth wave-guide. The time correlation between two-outstation waveform defines an ATD. The computed ATD represents locations with same time difference between two outstations. Those locations approximately define hyperbolas over the earth's surface. The intersection of several ATDs (hyperbolas) from a sferics candidate defines a fix location. The STARNET configuration has five receivers located in West Greenwich RI, Fairfax

VA, Hunstville AL, Miami FL and San Juan PR as shown in Figure 1. The following subsections present a review of the STARNET instrumentation and sferics location software.

2.1 STARNET Instrumentation

The instrument system can be separated in two parts: a number of receivers and a central computer station. A simplified sketch of this system is illustrated in Figure 2. Each receiver consists of an outside VLF antenna and preamplifier, a GPS timing generator and signal converter, and an inside personal computer (PC) with Internet communication access. The central computer station runs on a PC, which receives via Internet in a digital form the electric field signal measured by each receiver.

A more detailed diagram of the antenna receiver's components is shown in Figure 3. The VLF signal is pre-amplified at the antenna located outside the building some 30 meters or more to avoid electrical noise. In a nearby converter box the signals are synchronized to GPS time and encoded by Analog-to-Digital (A/D) converters. The digitized data are then sent inside to a PC with a Digital Signal Processor (DSP). The PC executes the identification algorithm that detects a probable sferics candidate and then sends compressed files to the central station over the Internet. The receiver hardware has a dynamic range exceeding 100 dB with a typical noise floor of 60 nano-Volts/meter/root-Hertz RMS. The pulse shape sampling interval is 102.4 microseconds with a timing accuracy within one microsecond of GPS time.

2.2 STARNET Software Overview

The system software is divided between the receivers and the central station. The receiver signal processing algorithms are optimized to separate distant, and therefore weak, sferics from

the interference that surrounds them. Signal quality control is integrated across the system to eliminate low-quality sferics data that could cause false location reports.

The receiver software is capable of capturing 70 sferics-per-second. The receiver bandwidth is defined by a finite impulse filter (FIR) digital filter extending 3.0 kHz above and below its center at 9.8 kHz. Each sferic waveform is contained in 13.1 millisecond windows. The wave-shape information is heavily compressed to about 160 bits per sferic. This compressed sferic data are accumulated into files of 16 seconds duration, which have a typical size of 5 to 20 kilobytes. These files are backed-up and transmitted to the central station. Once the data reaches the central station two tasks are performed: (a) Decompression and correlation, and (b) locating and optimization. In the decompression task each file is uncompressed and the waveform signal is restored. It follows that same source candidates observed in the different outstations are compared to extract the corresponding ATD values, as presented by Lee (1986a, 1986b). Namely, the 13.1 milliseconds waveform signal from two receivers are analyzed and the time lag with the highest cross-correlation value defines an ATD. Accordingly, ATD values are computed for all possible combinations of receiver pairs. In the present system with five receivers, ten ATD values are computed. As mentioned earlier, these ATD values represent positions between two outstations with a given signal arrival time difference. The intersection between those ATDs fixes a sferic location.

In the second task, Lee's (1986a) ATD technique serves as the primary locating algorithm. This approach minimizes the residuals in the ATDs, as expressed below:

$$\chi^2 = \frac{1}{N-2} \sum_{i=1}^{N_{ATD}} \frac{ATD_i^{simulated} - ATD_i^{measured}}{\sigma_i}^2 \qquad (1)$$

where N is the number of measured ATDs ($ATD_i^{measured}$), while $ATD_i^{simulated}$ represents the i^{th} simulated arrival time difference for a selected location, and σ_i is the standard deviation value for the i^{th} simulated ATD. For the five STARNET sensors configuration, ten ATDs are computed. This represents the combination of five receivers taken two at a time. The values of σ_is for the different regions on earth can be evaluated theoretically, or through comparisons against more definitive lightning measurements, such as the National Lightning Detection Network (NLDN), Cummins et al. (1998).

This method consists in finding an optimal position over the earth's surface that has the minimum χ^2. In order to retrieve this minimum residual value the algorithm computes simulated ATDs that are the expected ATDs at several locations over the globe. In general, this calculation follows as: 1) define a position over the globe that has a latitude and longitude; 2) compute the geodesic distance between this defined position and the different sensors; 3) compute the different ATD combinations, which are the distance difference between two outstations divided by the phase velocity (for simplicity we assume a single phase velocity equal to the speed of light); 4) compute the χ^2 residual as in equation (1); 5) repeat process 1 through 4 for several locations over the earth's surface; and 6) find the minimum χ^2 that represents the final location.

The procedure is illustrated in Figure 4 that shows two examples of lightning retrieval, one for an electrical discharge located in the United States, Figure 4a, and the other in South America, Figure 4b. Note that the hyperbolas intersect over the lightning source. At these locations the residual χ^2 is minimum. The computed χ^2 for the two cited examples are illustrated in Figures 4c and 4d, respectively. The shaded gray scale shows low values of χ^2 for lighter colors (white), and higher residuals for darker color region (dark gray). In those particular

examples the ATD residuals were zero at the lightning strike locations, assuming the same variance for all ATD pairs. Nevertheless, small errors in the evaluated ATD values, or small variations in the phase velocity may significantly enlarge the region for the possible electrical discharge. False fixes are avoided with at least four receivers. In the case presented in Figure 4d, if only three pairs of ATDs had been used, which represents a three-sensor configuration; two solutions would have been possible. This false position has a residual of 136,372 ms^2. Whereas the residual errors, for a five receivers configuration, near the actual position of the lightning strike yield residuals less than 3 ms^2.

All the ATDs for a same-source candidate are examined to estimate the strike location and time using a least-squares fit weighted selectively to certain ATDs. The algorithm adaptively compensates for correlation ambiguities, a problem that increases with long propagation distances. This is a consequence of the distortion of the electrical signal traveling the differing propagation paths to the receivers and possible different sferics noise observed at the same time. These effects distort the waveform and therefore create several ambiguous peaks. A final optimization takes into account the likely errors associated with each ATD in light of the estimated location and is dependent on the network layout. Proper resolution of these ambiguities is an important task as it increases the system accuracy and sensitivity especially at long distances.

3. Lightning Location Error Analysis

In the present study only the final position fixes of sferics measurements were available. These consisted of the latitude, longitude, time of occurrence, and some quality control

parameters of the sferics location fix. Unfortunately, measurements such as raw ATDs and sferics waveforms were not available. Consequently, any improvement in the lightning location had to rely on empirical and experimental corrections based on theoretical effects that can degrade the accuracy of these measurements. These effects are the estimated ATDs, and the spatial configuration of the radio receivers.

As the VLF sferics electric field signal propagates through the earth-ionosphere wave-guide to the radio receivers, the signal interacts with the bounded medium and attenuation occurs. Changes in the ionosphere properties attenuate the electric field in addition to delaying or speeding up its phase velocity. Consequently, propagation produces distortion in the electrical waveforms. The attenuation depends on the surface background of propagation (different ground conductivity for land or water), changes in ionosphere's height during day and night times, and finally the propagation direction (e.g., east-west, west-east, south-north and north-south).

In addition to attenuation effects, there are variations in the phase velocity between the sferics and the various receivers. Phase velocity measurements compiled by Wait (1961), Al'pert and Fligel' (1970) and Taylor (1960) at 10 kHz showed values of 1,05 and 1,02 of the speed of light for day and night propagation respectively. Lee (1986a) on his experimental VLF ATD network in Europe has computed the multipliers of the speed of light ranging from 1.001 to 1.007 that depend on the region of the sferics measurements. Minimum values of the residual errors on his ATD method indicated an optimal constant of 1.004. The STARNET system uses a constant daytime phase velocity of 1.0025 of the speed of light, while during nighttime it applies a ratio of 1.0055.

The ATD values, which are calculated in the signal processing by applying a cross-correlation of the pulse shape (electrical signal), are expected to have random errors associated with this signal analysis. Additionally, the change in the phase velocity and signal strength that is attenuated during its propagation contributes to deform the sferics waveform. This effect will induce other inherent errors in the signal processing. Very small ATD errors may produce erroneous lightning locations, which depend on the range and relative location of the receivers with respect to the lightning sites. Figure 4c and 4d show minimum ATD residuals that depend on ATD errors optimal solutions, which are difficult to locate due to the enlargement of a minimum residual area. Lee (1990) on his bias elimination study has found that ATDs biases were a function of receivers' location and the lightning strike position. Unfortunately, the removal of any ATD bias is dependent of the availability of the raw ATD measurements.

The ATD method presented in section 2.2 can be treated as a geometry problem in a first order solution. In that problem, the ATDs intersect in a region and define an optimal position for the lightning strike. Unfortunately, the spatial distribution of the radio receivers contributes to define regions where the ATD hyperbolas, as presented on Figure 4a and 4b, become parallel. In the absence of ATD errors a sferics fix is always found with a configuration of at least four receivers. Free ATD error measurements are very difficult to be accomplished. Consequently, an area that represents the minimum residual defines the ATD solution that is enlarged by the receiver's baseline where the ATD hyperbolas become parallel. A feasibility study can diminish such problems. In this experimental phase of STARNET, the location of the receivers was determined by the availability of suitable infrastructure consistent with broad area coverage.

This section analyzes the lightning location error in the ATD method applied by STARNET for its present configuration. First, the expected spatial location error distributions

are computed through numerical simulations assuming known existing errors in the system. Secondly, the relative location error distribution is estimated using the National Lightning Detection Network (NLDN) over the continental US and the Lightning Imaging Sensor (LIS) that measures lightning over the tropics. Finally a tentative explanation of the location errors and subsequent corrections are investigated.

3.1 Simulation of location error: Random ATD errors

The ATD method presented in section 2.2 can be applied to retrieve expected location errors assuming that ATD errors are random. This means that actual and measured ATD values are free of systematic differences. This assumption is made in truancy of raw ATD measurements. Time accuracy and identification of the correct peak in the signal-processing algorithm can be attributed to produce random errors. STARNET uses GPS timing to stamp the electric field waveforms with an accuracy of 1 μsec. An internal clock used with the GPS produces this time resolution that can vary randomly. The distortion of the waveform caused by the propagation in the earth-ionosphere wave-guide can interfere with the identification of the proper peak in the cross-correlation analyses. Residual checks conducted by RDI (not shown herein) revealed a 5-10 μsec error standard deviation in the ATD calculations. This random error in ATD evaluation can introduce both systematic and random errors in lightning location. In this study, a conservative 15 μsec ATD error standard deviation was used to account for the RDI recommended value and other uncertainties unknown at the present moment. More accurate specification of ATD error statistics requires extensive use of raw ATD values and the sferics electric field waveform measurements, which can be the subject of future studies when new data become available.

A Monte Carlo simulation experiment was conducted in an effort to statistically evaluate the lightning location error characteristics associated with the above sources of uncertainty. The first error source, namely ATD detection error (ε), is defined as a Gaussian random variable with zero mean and 15 μsec standard deviation (σ_ε). Assuming constant phase velocity an ATD error (Ψ) is defined as follows:

$$\Psi = \sum_{i=1}^{10(pairs)} \left[\hat{ATD}_i - ATD_i \right] = \sum_{i=1}^{10(pairs)} \left[\{ATD_i + \varepsilon\} - ATD_i \right] \quad (2)$$

where $\hat{ATD}$ and ATD are the measured and true arrival time differences. For an independent ATD errors (ε) the variance (σ^2) of variable χ can be expressed as:

$$\sigma^2 = N\sigma_\varepsilon^{\,2} \quad (3)$$

Using the 95% confidence bounds associated with variance σ^2 one can delineate the corresponding probable positions of lightning occurrence in space (or else called error ellipses). Using these theoretical calculations bi-normal probability distribution functions of lighting location error can be derived. Similar error distribution functions can be derived experimentally using as reference lightning measurements from more definitive but localized lightning network observations (this is discussed in section 3.4). Figure 5 shows the estimated mean location error of STARNET for the current configuration of its sensors, a 15 μsec ATD detection error standard deviation, and constant phase velocity ($3x10^8$ ms^{-1}). It is noted that the mean location error becomes significant at sensor ranges further than 3,000 km. Regions with high error gradients are associated with the parallel isochrones effect mentioned in section 3. This geometric effect could be overcome by locating sensors at the boundaries of a polygon.

3.2 Relative location error

The expected location errors presented in Figure 5 are subsequently compared against an experimental error analysis based on "ground truth" data. Coincident lightning measurements from the US National Lightning Detection Network (NLDN) (Cummins et al., 1998) and STARNET have been compiled for the period of July 13 to 29, 1997 and December 1, 1997 through February 28, 1998. Additionally, coincident measurements from the Lightning Imaging Sensor (LIS) (Christian et al., 1999) on board the Tropical Rainfall Measuring Mission (TRMM) satellite (Simpson et al., 1988, Kummerow et al., 1998) were gathered during the period of December 1, 1997 through February 28, 1998. These compiled "ground truth" benchmark data sets are used to obtain the relative spatial distribution of errors over the continental US, the North Atlantic Ocean and South America.

The first data set period within the summer season exhibits significant lightning activity over the continental US. The second period shows summer storms activities in the South America and winter storms characterized by frontal systems over the continental US that propagate through the North Atlantic Ocean. The NLDN system has an expected detection efficiency of about 80-90% for cloud-to-ground flashes, and an accuracy of location ranging between 0.5 and 2 km within the continental US (Cummins et al., 1998 and Idone et al., 1998a and 1998b). These error estimates were retrieved at a few locations over the eastern US near the receivers. Thus, their application to other regions of NLDN coverage is still subject to more analyses. The LIS location error or expected uncertainty is 6-8 km (accounting the true location of a flash versus LIS pixel resolution; at nadir where the pixel resolution is 4km LIS error is 1.5 pixels). Consequently, the errors computed herein are subject to the accuracy of the herein considered "ground truth".

STARNET sferics were matched with NLDN and LIS coincident measurements. In this procedure, lightning flashes from NLDN and LIS are compared to STARNET sferics. Flashes are commonly defined as a group of several strokes (usually 1-4) within a radius of 10-100 km and a time window of 0-400 milliseconds while strokes are the result of the electrical field break down. A total of 858,671 STARNET-NLDN and 723 STARNET-LIS matched flashes have been compiled for this error analyses. A match was only defined when the candidate sferics/flash pair was detected by both systems within a 1 and 100 milliseconds time window for NLDN and LIS respectively, and was within the same region of measurements (i.e. within a radius of 300 km). Subsequently, erroneous flashes/sferics matches were discarded from the analysis. The difference between the two time windows for searching a lightning match is based on the characteristics of the different instruments. NLDN measures mainly CG lightning in a wideband receiver (1-500 kHz) system that covers the small fraction used by STARNET. Therefore, some of the observed lightning sources ought to be measured by both systems almost in the same time. The LIS system measures the optical signal created by a lightning strike. In principal this instrument measures both CG and IC events. Since the information of CG and IC and flash duration were not available and due to the low observation frequency of LIS measurements, a wider time window was used to produce a higher number of potential matches and account for the different instrument characteristics.

Figure 6 shows the mean location error derived from the matched sferics/flash pairs for 1 by 1 degree boxes over the continental US and 2.5 by 2.5 degrees elsewhere. The location error is defined as the absolute difference between STARNET and NLDN/LIS lightning locations. Comparing the above data-based mean error patterns against the simulation results shown in Figure 5 one can see notable differences, especially in the magnitude of the range dependent

variation of the mean error towards the West Coast of US. Over the North Atlantic Ocean and west of South America the observed errors are within the simulated errors shown in Figure 5. Northeast US and the Caribbean region show higher relative errors, which is primarily due to the increased NLDN uncertainty. NLDN analyses of the chi-square values for the coincident matches at these locations show STARNET errors ranging from 10-50 km.

The increased errors in the west coast of US indicate potential biases in the ATD measurements likely associated with the use of erroneous phase velocity values. Direct inspection of the ATD bias as performed by Lee (1989) is compromised due to the absence of raw ATD measurements. Instead, the effect of phase velocity modeling deployed by STARNET is investigated as an inherent error source on the STARNET location algorithm.

3.3 Phase velocity analysis

In order to account for the phase velocity error in the simulation framework, the theoretical error ellipses location model (Ψ) of equation (2) is modified as following:

$$\Psi = \sum_{i=1}^{10(pairs)} \left[\hat{ATD}_i - ATD_i \right] = \sum_{i=1}^{10(pairs)} \left[\left\{ \frac{ATD_i}{c_1} + \varepsilon \right\} - \frac{ATD_i}{c_2} \right] \tag{4}$$

where c_1 and c_2 are the multiplicative scale factors of the speed of light representing the modeled and actual phase velocity mean (independent of time and geographic location) deviation from the speed of light. These parameters are evaluated by minimizing the difference between simulated and data based determined mean location errors. The procedure is as following. For a NLDN location matched with STARNET, a propagation model is applied to determine the ten STARNET ATD values assuming a phase velocity, c1. The NLDN strike location is considered as the true value. Independent additive random error, represented by normal distribution with

zero mean and standard deviation of 15 μsec, is added to the modeled ATD values. These ATDs are ingested in a locating algorithm that uses a hypothetically erroneous phase velocity value (i.e., c2). The final lightning location is compared with the location of the actual STARNET match. This procedure is repeated for the whole matched data set and for various c1 and c2 configurations. The optimal c1 and c2 selection is the one providing the best resemblance of the mean error distribution shown in Figure 6. From the current analysis the optimal values for c_1 and c_2 are 1.004 and 1.0039 respectively, which shows an overall phase velocity modeling error of 0.01%. Having determined c1, c2 and the ATD random error standard deviation the above model can be used to derive theoretical error ellipses for the STARNET lightning location estimates.

Figure 7 shows the mean location error isochrones (blue solid contours) and error ellipses for 5^o latitude/longitude intervals derived from this simulation experiment between 20-50N latitude and 125-60W longitude. The red and yellow error ellipses correspond to unbiased and biased (i.e., western and northwest/northeast bias in western and northern locations, respectively) estimates, accordingly. The simulation using Equation (4) shows that some regions are consistent (east coast, Texas, Northern planes) with the experimentally derived errors shown in Figure 6. In the west coast the error shapes are dissimilar, but the magnitudes are comparable. Note that the main tendency apparent in both simulations and data is that in the west coast sferics are computed further west than their actual location. The orientation of error in the US mid-west derived from data (Figure 6) is not well represented by the present simulation, which indicates that error sources depend on the distances to the receivers in a way that Eq 4 fails to do.

3.4 Sferics Location Error Correction

A statistical model is developed for STARNET sferics location error estimation using varying "ground-truth" measurements. Over the continental US the evaluation is performed using the National Lightning Detection Network (NLDN) measurements. Over the Atlantic and Pacific oceans, as well as the South America region, the error model is evaluated using LIS measurements. The sferics location error model combines the theoretically derived error ellipses, described in the previous section, with a spatial probability density function of sferics location errors and information from geo-stationary satellite cloud top IR temperature.

The spatial distribution of sferics location error is modeled using bi-normal probability density function (PDF) of the following form:

$$f(\lambda,\varphi)=\frac{1}{2\pi\sigma_\lambda\sigma_\varphi\sqrt{1-\rho^2}}\exp\ \frac{-1}{2\left(1-\rho^2\right)}\ \left[\frac{\lambda-\bar{\lambda}}{\sigma_\lambda}\right]^2-2\rho\ \frac{\lambda-\bar{\lambda}}{\sigma_\lambda}\ \frac{\varphi-\bar{\varphi}}{\sigma_\varphi}\ +\ \left[\frac{\varphi-\bar{\varphi}}{\sigma_\varphi}\right]^2 \qquad (5)$$

where λ and φ are joint random variables representing the Longitudinal and Latitudinal location error measured in distance (in km) from a STARNET estimated sferics location, while $\bar{\lambda},\bar{\varphi}$ and $\sigma_\lambda,\sigma_\varphi$ are the corresponding mean and standard deviation values, and ρ is their cross-correlation value for a certain location on earth which determines the angle of the major axis with respect to the latitude-longitude coordinates. These parameter values may be evaluated experimentally for specified regions on earth based on available STARNET sferics and "ground truth" flash matches.

Figure 8 shows an example of spatial frequency distribution plots of the STARNET sferics location errors compared to NLDN and LIS lightning data sets, binned in 2.5-degree

square boxes. The circles/ellipses have radii of 300 km around the center of the grid boxes. The different points in the scatter plots correspond to location errors represented in polar coordinates (i.e., azimuth and distance), while colors are used to show the respective frequency of occurrence. In addition to these azimuthal distributions, we have selected four locations over the west, central, and east US, and northern South America to show the error frequency distribution along the main axis of the error ellipse as a function of distance from the grid point. It is apparent that the location error distributions for the Eastern United States area and part of the Atlantic Ocean are mainly random with zero spatial correlation (i.e., no azimuth orientation) and zero mean (i.e., no bias). On the other hand, in the central and western part of the US the location errors tend to concentrate along certain directions, and there is an obvious westerly bias (i.e., STARNET estimated sferics locations tend to be west of their actual location). The 2D histograms show that the location error distribution may be well represented by a bi-normal PDF (equation 5). Consequently, in the location error model the bi-normal PDF parameter values were determined separately for every 1x1 degree grid within the continental US where NLDN is the reference data source, and 2.5x2.5 degree grid elsewhere with LIS as reference.

In summary, the STARNET location error model includes the following processing steps: (1) delineation of the area of possible location errors from the theoretically derived error ellipses (i.e., the Monte Carlo simulation represented by Equation 4), and (2) statistical determination of the correction to be applied to the STARNET sferics location estimates. The second step uses a combination of the experimentally evaluated location error bi-normal PDF and GOES-8 IR brightness temperature observations of convective cloud tops within the error ellipse areas. Inspection on the histogram of IR brightness temperature values for pixels with lightning has shown that 90% of its area is under the -15 ^{o}C threshold. This value is also known to be the

temperature threshold beyond which water droplets freeze in a cloud system. Subsequently, the –15 ^{o}C isotherm is selected to delineate expected convective cloud areas within the error ellipses.

The flow chart of the proposed error correction scheme is shown in Figure 9. First, the method examines whether a STARNET estimated sferics location is in a region with expected mean error (see Figure 6) of less than 20 km and corresponding IR temperature below -15 ^{o}C. In that case the estimate is considered as a good fix. For any other STARNET estimate the procedure retrieves for its corresponding error ellipse area the spatial probability of the location errors according to the PDF evaluated for the specific region, and the IR brightness temperature distribution. A rank is performed according to the PDF values of the location misplacements that are under the –15 ^{o}C IR cloudiness area, and the misplacement with the highest PDF value is selected. In case of no area within the error ellipse with temperature below –15 °C the specific sferics datum is rejected.

Figure 10 and 11 present typical examples of the above correction procedure on STARNET sferics estimates over the validation period**.** These figures show a comparison between STARNET and combined LIS and NLDN data sets for July 20 1997 at 00:15 UTC, and January 8 1998 at 09:45 UTC. The top panels show STARNET without correction, the middle panels show NLDN and LIS, and bottom panels show STARNET after location correction is applied. It can be noted that regions where STARNET errors are small no changes are observed. Figure 10 shows an example of STARNET misplacement further west in the west coast. The correction procedure is able to reposition the lightning fix eastward over the clouds, which is shown to agree with NLDN measurements. Figure 11, where LIS data is also available, shows a squall line moving towards Florida and South Carolina. Note that almost no significant location changes are observed and sferics measurements coincide with NLDN and LIS observations. At

the western South America, the sferics strips are relocated around the convective systems observed in that region, while over the Atlantic ITCZ the sferics are repositioned along the cold clouds. Figure 12 shows the overall mean location error of STARNET with respect to NLDN for the periods of July 13-29, 1997 and December 1997 through February 1998 over the continental US. The main observation from this figure is that applying the proposed correction: (1) there is a considerable reduction in the magnitude of the error over the central and western US; and (2) the spatial distribution of errors becomes random (i.e., no systematic range dependent differences are observed). Note that in the eastern part of the US the errors remain insignificant. Further demonstration of the location error reduction is presented using the cumulative distribution function (CDF) of errors for different locations of the US. Figure 13 shows the cumulative error distributions for areas east (left panel) and west (right panel) of 90W. Note that the east coast error CDF is insensitive to the error correction. On the other hand, the west coast error CDF shifts significantly to lower values. For example, at 20 km error range the original sferics data would represent only 40% of the cumulative probability, while after correction this range represents nearly 80% of the total.

4. Conclusions

A new experimental network (STARNET) of five ground-based radio receivers located along the US east cost and Puerto Rico has been briefly described. A sferics location error analysis and a correction scheme are also presented. A total of three and a half months of coincident STARNET and NLDN data over the continental United States, as well as STARNET and TRMM-LIS data over the Atlantic Ocean and other regions of North and South America were used in this research.

The location error analysis was conducted through Monte Carlo simulation based on theoretical error considerations and compared to relative error location using NLDN and LIS measurements as "ground truth". The first simulation applied a conservative 15 μsec random ATD error standard deviation that would account for random effects by distortion of the sferics waveform, phase velocity variations, timing stamp uncertainty and receivers spatial configuration. The simulation experiment showed a spatial distribution of location error of the order of 100 km over distances greater than 3,000 km from the receivers. Comparison with the mean error distribution retrieved from NLDN and LIS data showed good agreement over the central and eastern coast of US (errors below 20 km), North Atlantic ocean (errors between 10-50 km), Caribbean (errors below 20 km) and western South America (errors between 20-50 km). The western region of US showed differences in location error magnitudes and orientations.

It was argued that phase velocity parametrization is the main candidate for investigating this westward sferics displacement bias. Simulation was performed to evaluate error in phase velocity that in combination with a 15 μsec ATD random standard deviation error would best explain the displacement errors in the matched NLDN and STARNET data set. The simulations showed a 0.01% error in modeling the phase velocity. Accounting for the above phase velocity deviation and the random ATD error we were able to explain the westerly displacement of bias over the West Coast, but could not fully reproduce its orientation. ATD biases exist due to propagation of the sferics signal in the earth-ionosphere wave-guide and unlike the assumptions of the present analysis, they depend on the lightning strike and relative location of the receivers.

A location error correction fix was developed that combines the theoretically derived error ellipses with a statistical location error model, evaluated based on a calibration set of NLDN/LIS and STARNET data, and coincident satellite IR brightness temperature data.

Evaluation of corrected sferics locations over the continental US showed a 40-50% location error reduction in the western part of US. These relative location errors are below 50 km and shown to be randomly distributed. In the East Coast the errors remained well below 20 km.

The experimental STARNET system presented herein is no longer operational. A new experimental network based on the same principles is being deployed in Europe with expected activation the summer of 2001. The network will consist of six stations located in Larnaca (Cyprus), Mt. Etna (Italy), Evora (Portugal), Birmingham (UK), and Iasi (Romania), and will set the ground for further development in the direction of VLF lightning monitoring.

Acknowledgements: We acknowledge and appreciate discussions and input from Dr. Steve Goodman of NASA/MSFC, and Dr. Earle Williams of MIT. This research used sferics data from the Sferics Timing and Ranging Network (STARNET) implemented by Resolution Displays, Inc., under funding by NASA Small Business Innovative Research grant (NAS5-32825). We also are grateful to Dr. Ramesh Kakar, Code Y at NASA Headquarters, for his encouragement and support. This study was supported by NASA New Investigator Program award under grant NAG5-8636. The first author was also supported by the Conselho Nacional de Desenvolvimento Científico e Tecnológico (CNPq) under grant 260133/93.0 of the Brazilian government.

5. References

Al'pert, Ya. L. and D.S. Fligel', 1970: Propagation of ELF and VLF waves near the earth, Consultants Bureau, New York-London, 171pp

Baker, M.B., H.J. Christian, J. Latham, 1995: A computational study of the relationships linking lightning frequency and other thundercloud parameters, Q. J. R. Meteorol. Soc., 121, 1525-1548.

Budden, K.G., 1951: The Propagation of a Radio-Atmospheric. Phil. Mag., Ser 7, 42, 1-19.

Christian, H.J., R.J. Blakeslee, S.J. Goodman, D.A. Mach, M.F. Stewart, D.E. Buechler, W.J. Koshak, J.M. Hall, W.L. Boeck, K.T. Driscoll, and D.J. Boccippio, 1999: The Lightning Imaging Sensor. Proccedings of the 11th Int. Conf. on Atmos. Electricity, Guntersville, Alabama, 746-749.

Cummins, K., M. Murphy, E. Bardo, W. Hiscox, R. Pyle, and A. Pifer, 1998: A combined TOA/MDF technology upgrade of the U.S. National Lightning Detection Network, J. Geophys. Res., 103, 9035-9044.

Idone, V.P., D.A. Davis, P.K. Moore, Y. Wang, R.W. Henderson, M. Ries, and P.F. Jamason, 1998a, Performance evaluation of the U.S. National Lightning Detection Network in eastern New York, 1: Detection efficiency, J. Geophys. Res. 103, 9045-9055.

Idone, V.P., D.A. Davis, P.K. Moore, Y. Wang, R.W. Henderson, M. Ries, and P.F. Jamason, 1998b, Performance evaluation of the U.S. National Lightning Detection Network in eastern New York, 2: Location accuracy, J. Geophys. Res. 103, 9057-9069.

Kummerow, C., W. Barnes, T. Kozu, J. Shiue, J. Simpson, 1998: The Tropical Rainfall Measuring Mission (TRMM) Sensor Package. Journal of Atmospheric and Oceanic Technology: **15**, 809–817.

Lee, A.C.L., 1986a: An experimental study of the remote location of lightning flashes using a VLF arrival time difference technique, Quart. J. R. Met. Soc., 112, 203-229.

Lee, A.C.L., 1986b: An operational system for the remote location of lightning flashes using a VLF arrival time difference technique, J. Atmos. and Ocean. Tech., 3, 630-642.

Lee, A.C.L., 1988: Precise long-range lightning mapping with the UK arrival time difference VLF technique. NOAA Special Report: Proc. of the 1988 International Aerospace and Ground Conference on Lightning and Static Electricity, 425-433.

Lee, A.C.L., 1989: The limiting accuracy of long wavelength lightning flash location, J. Atmos. and Ocean. Tech., 6, 43-49.

Lee, A.C.L., 1990: Bias elimination and scatter in lightning location by the VLF arrival time difference technique, J. Atmos. and Ocean. Tech., 7, 719-733.

Pierce, E.T., 1977: Atmospherics and Radio Noise, in Lightning, Ed. R.H. Golde, Academic Press, London, 351-384.

Simpson, J., J.R.F. Adler, and G.R. North, 1988: A proposed Tropical Rainfall Measuring Mission (TRMM) satellite. Bull. Amer. Meteor. Soc., **69**, 278-295.

Taylor, W.L., 1960: Daytime attenuation rates in the v.l.f. band using atmospherics, J. Res. Nat. Bur. Stand., 64D(Radio Prop.), 349.

Wait, J.R, 1961: A diffraction theory for l.f. sky-wave propagation, J. Geophys. Res., **66**, 1713-1724.

Figure Captions

Figure 1. Location of STARNET radio receivers.

Figure 2. Overview of STARNET network architecture

Figure 3. Sketch of STARNET antenna receiver's component.

Figure 4. Example of the ATD technique applied to a hypothetical lightning source. (a) ATD curves for a lightning discharge located over the central part of US; (b) same as (a) for the central part of South America; (c) the correspondent χ^2 residuals for the example (a); and (d) the same as in (c) but for example (b). The five STARNET stations produce 10 pairs of ATD isochrones, which correspond to each of the curves plotted in these two figures. The gray scale represents normalized minimum and maximum values of χ^2 residuals. Light colors (white) represent the minimum while dark ones (dark gray) shows the maximum values of ATD residuals. The isochrone labels on (c) and (d) represent 10*LOG10(χ^2).

Figure 5. Mean sferics location error associated with the STARNET ground receiver configuration, and a Gaussian random signal processing error with zero mean and 15 μsec standard deviation. Phase velocity was assumed constant in this simulation experiment. The STARNET receiver locations are designated by Δ and the state abbreviation.

Figure 6. Spatial distribution of STARNET mean relative location error, using NLDN and LIS measurements as reference.

Figure 7. Simulated mean location error isochrones (blue contours) and error ellipses for the ATD error statistics described in Section 3. The red ellipses correspond to no bias, while the yellow to westerly (for the west coast locations) and northwesterly-to-northeasterly (for the northern locations) displacements.

Figure 8. Scatter plot of STARNET location error distributions in relation to NLDN and LIS for 2.5x2.5 degree boxes. NLDN matches are used over the continental US while LIS is used elsewhere. The colors represent the frequency of each azimuth/range error shown in the scatter plots. The circles/ellipses represent a radius of 300 km around the center of the grid box. The number at the top of each circle represents the number of matching sferics/flashes observed in that grid box. The four histograms present the frequency of occurrence along the main axis of error distribution for specific points over the west, central and east US, and Colombia South America.

Figure 9. Flow chart of the STARNET sferics location error correction scheme.

Figure 10. Spatial distribution of lightning as measured by NLDN and STARNET on July 20 1997 at 00:15 UTC superimposed with GOES-8 Infra-Red images. Top panel, shows STARNET without correction. Middle panel shows correspondent NLDN measurements and bottom panel shows STARNET data after location correction is applied.

Figure 11. Spatial distribution of lightning as measured by NLDN, LIS and STARNET on January 8 at 09:45 UTC (TRMM orbit 655) UTC superimposed on GOES-8 Infra-Red images. Top panel, shows STARNET without correction. Middle panel shows the corresponding NLDN (blue) and LIS(red) measurements and bottom panel shows STARNET data after location correction is applied.

Figure 12. Mean error distribution of STARNET compared to NLDN after the GOES IR image correction is applied.

Figure 13. Cumulative error distribution for the (left panel) east coast of US (east of 90W) and (right panel) west coast (west of 90W). The black curve shows the original cumulative distribution and the red line the CDF after the correction is applied.

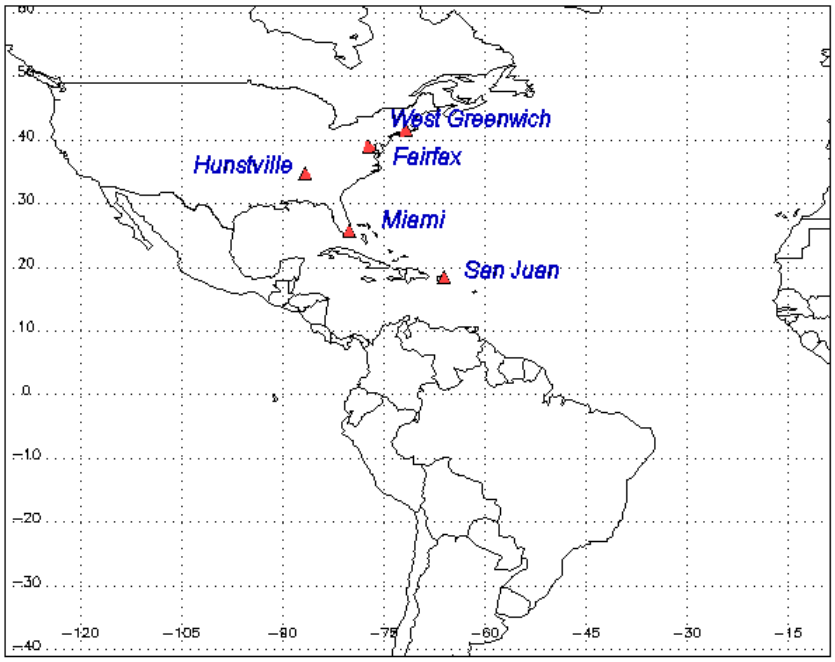

Figure 1. Location of STARNET radio receivers.

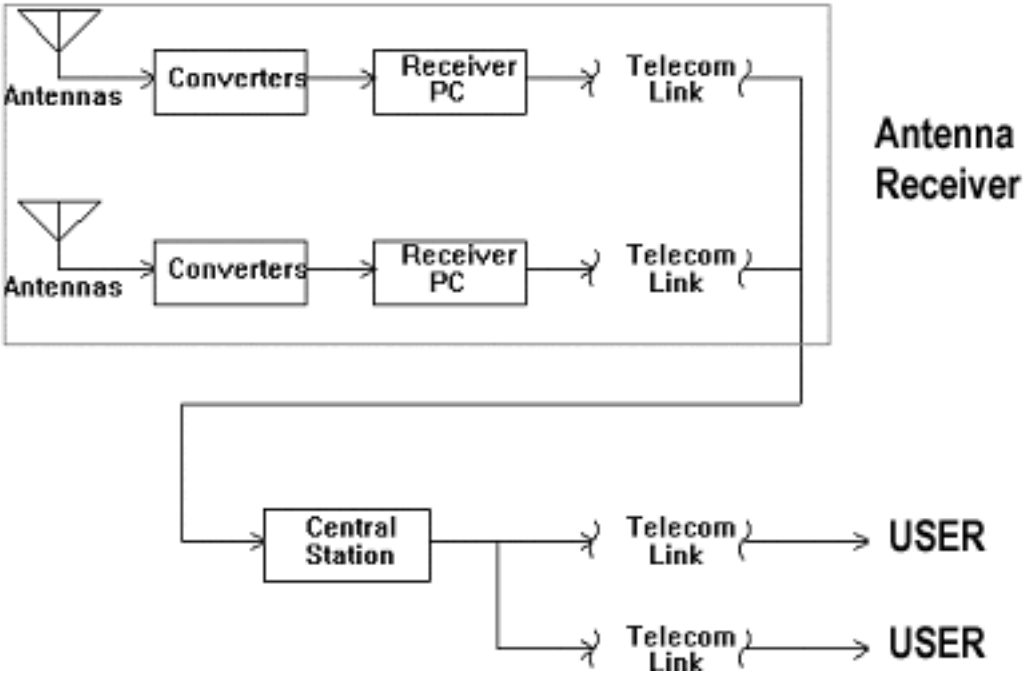

Figure 2. Overview of STARNET network architecture

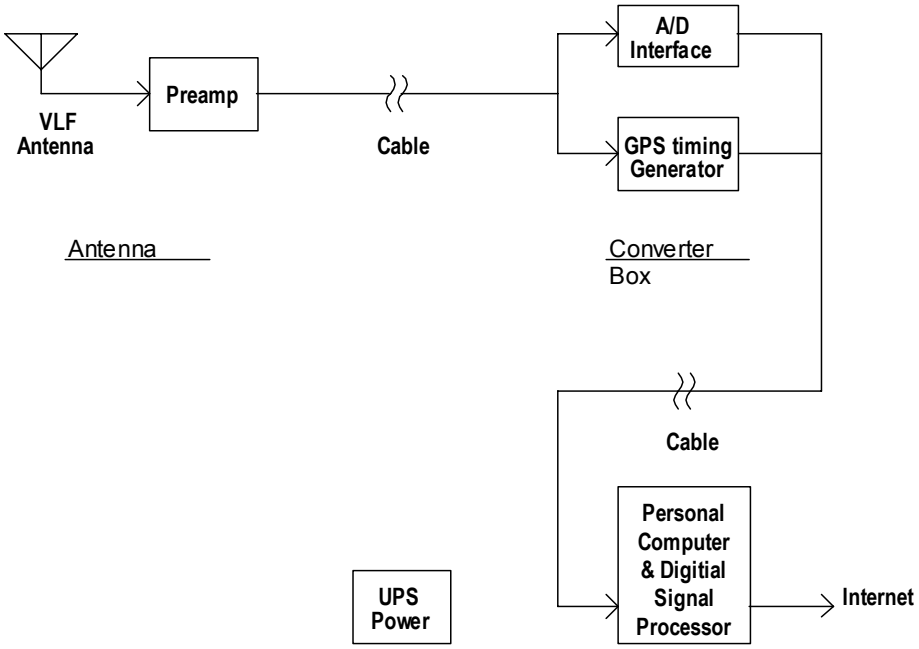

Figure 3. Sketch of STARNET antenna receiver's component.

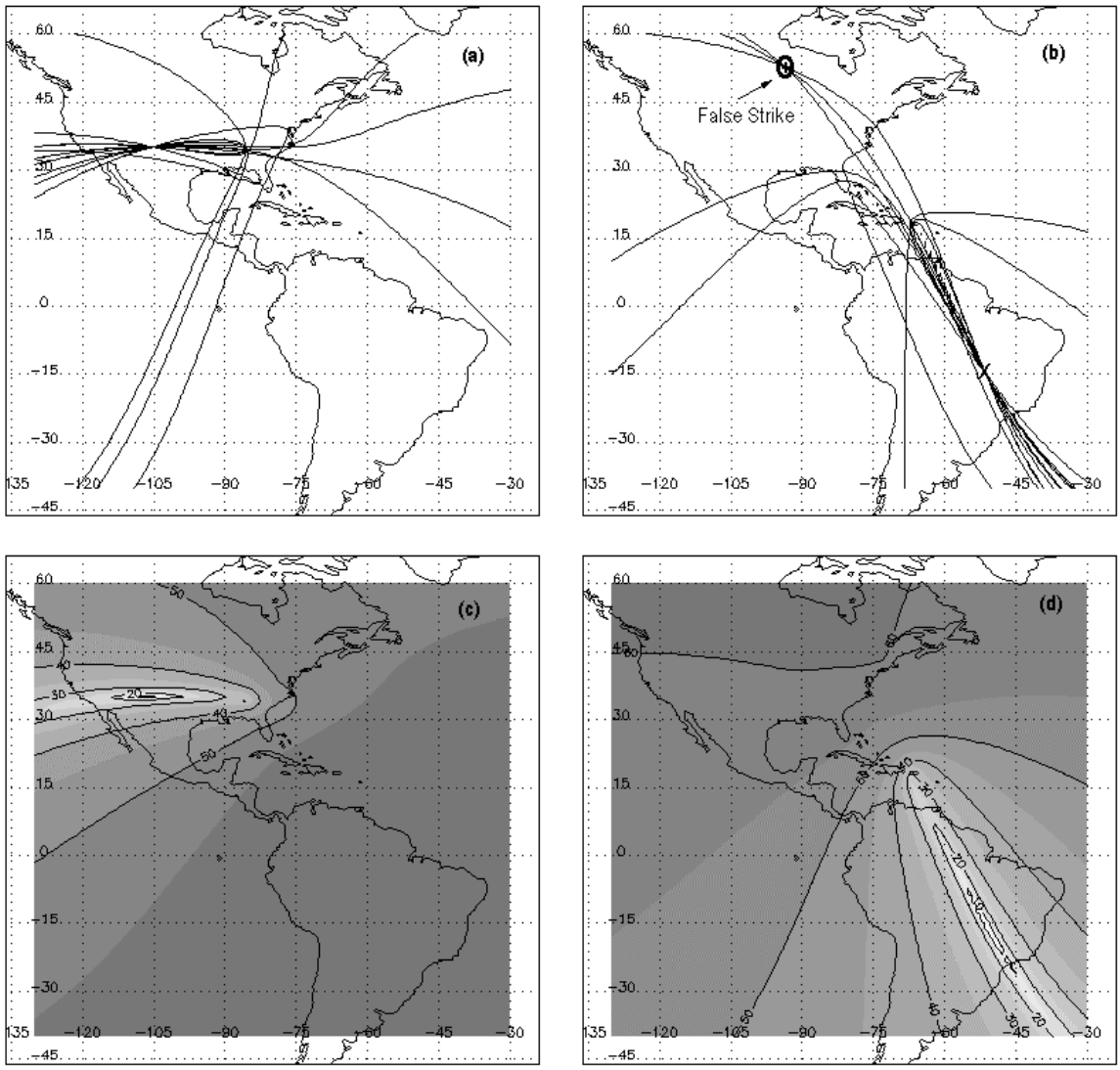

Figure 4. Example of the ATD technique applied to a hypothetical lightning source. (a) ATD curves for a lightning discharge located over the central part of US; (b) same as (a) for the central part of South America; (c) the correspondent χ^2 residuals for the example (a); and (d) the same as in (c) but for example (b). The five STARNET stations produce 10 pairs of ATD isochrones, which correspond to each of the curves plotted in these two figures. The gray scale represents normalized minimum and maximum values of χ^2 residuals. Light colors (white) represent the minimum while dark ones (dark gray) shows the maximum values of ATD residuals. The isochrone labels on (c) and (d) represent 10*LOG10(χ^2).

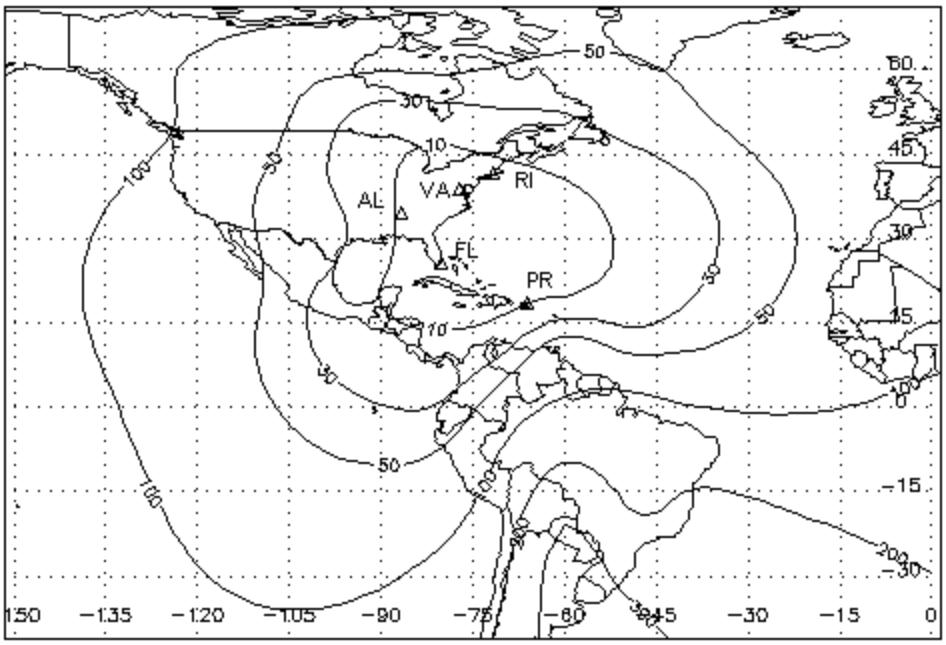

Figure 5. Mean sferics location error associated with the STARNET ground receiver configuration, and a Gaussian random signal processing error with zero mean and 15 μsec standard deviation. Phase velocity was assumed constant in this simulation experiment. The STARNET receiver locations are designated by Δ and the state abbreviation.

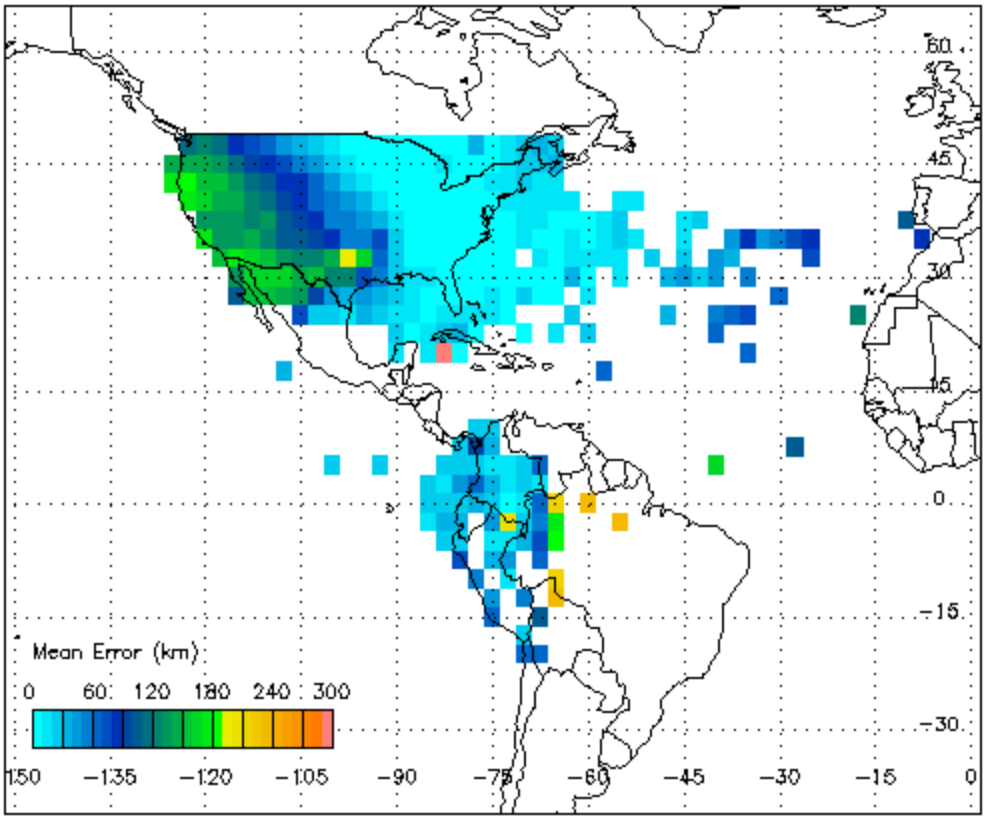

Figure 6. Spatial distribution of STARNET mean relative location error, using NLDN and LIS measurements as reference.

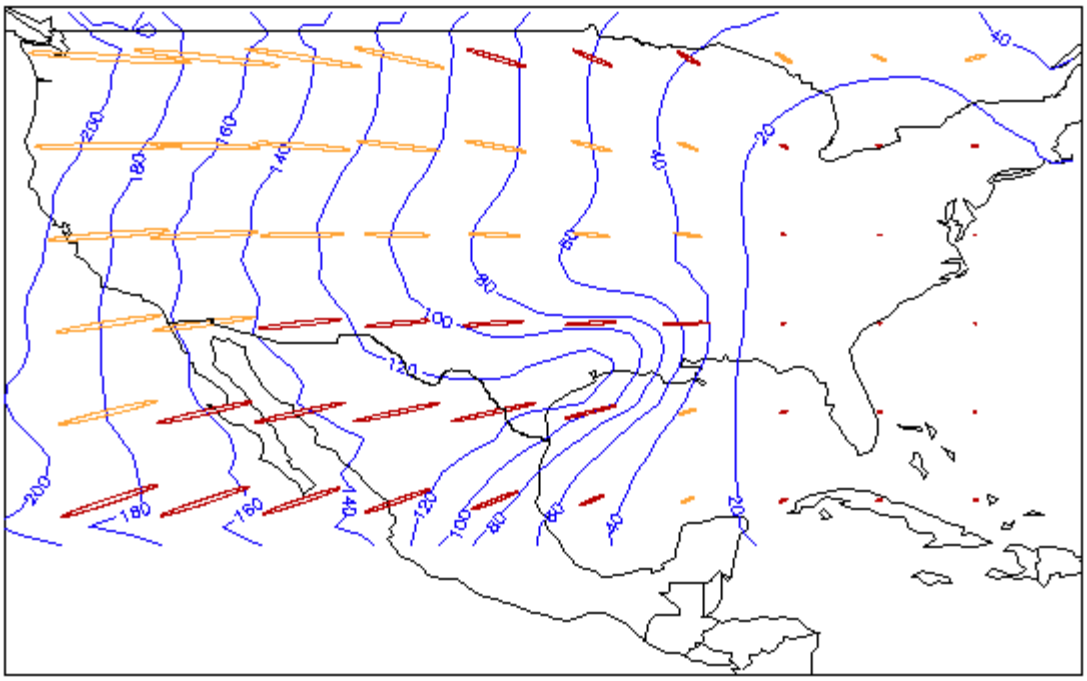

Figure 7. Simulated mean location error isochrones (blue contours) and error ellipses for the ATD error statistics described in Section 3. The red ellipses correspond to no bias, while the yellow to westerly (for the west coast locations) and northwesterly-to-northeasterly (for the northern locations) displacements.

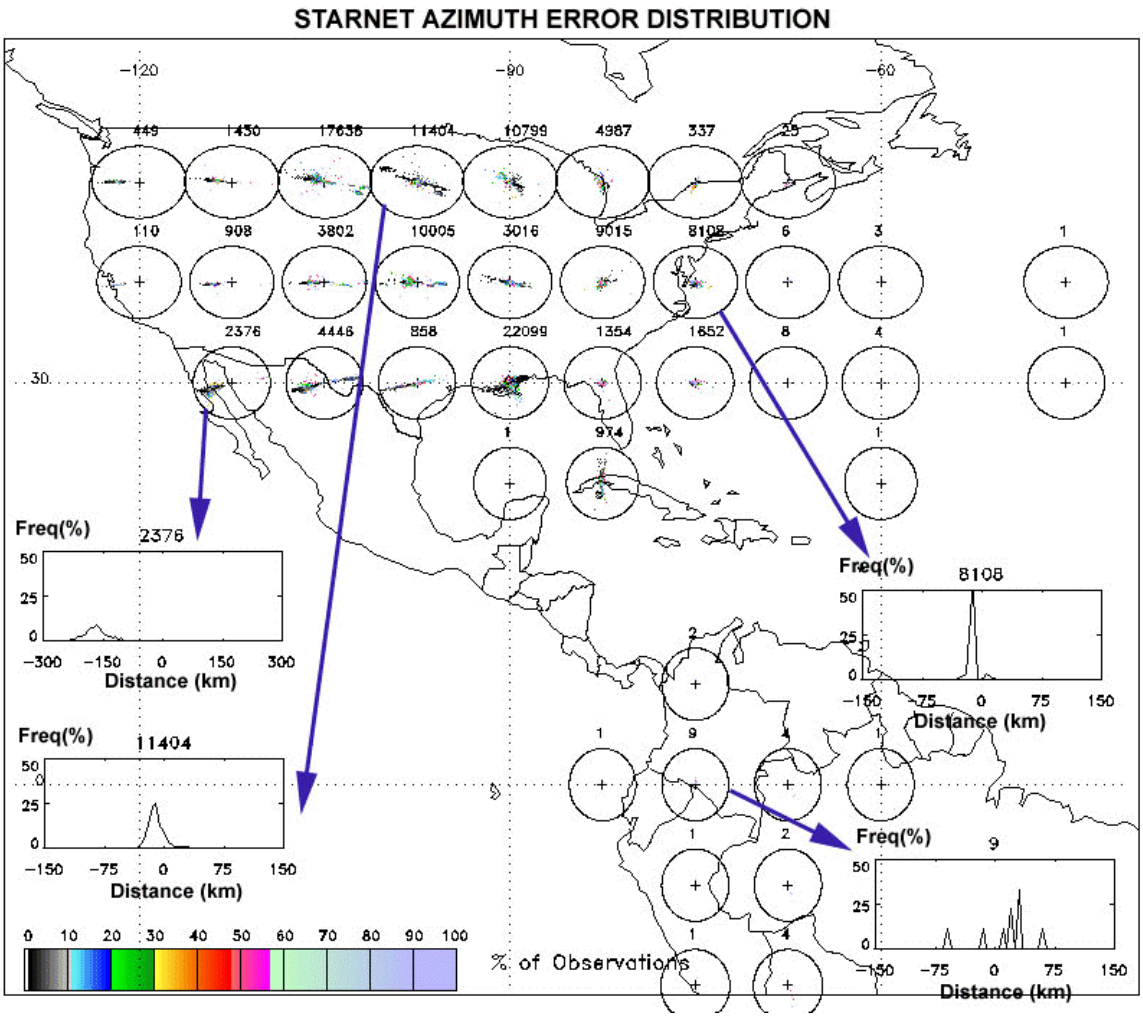

Figure 8. Scatter plot of STARNET location error distributions in relation to NLDN and LIS for 2.5x2.5 degree boxes. NLDN matches are used over the continental US while LIS is used elsewhere. The colors represent the frequency of each azimuth/range error shown in the scatter plots. The circles/ellipses represent a radius of 300 km around the center of the grid box. The number at the top of each circle represents the number of matching sferics/flashes observed in that grid box. The four histograms present the frequency of occurrence along the main axis of error distribution for specific points over the west, central and east US, and Colombia South America.

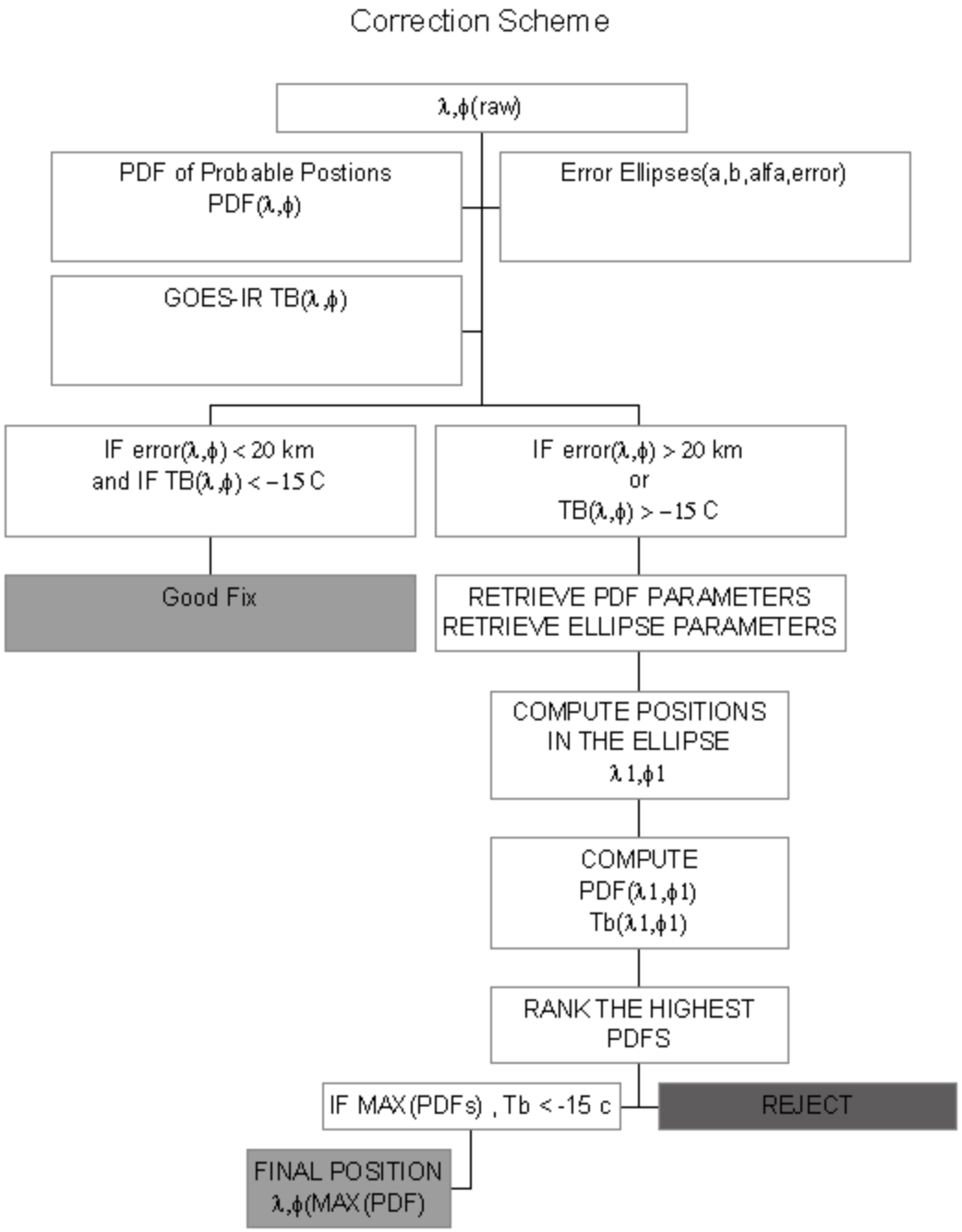

Figure 9. Flow chart of the STARNET sferics location error correction scheme.

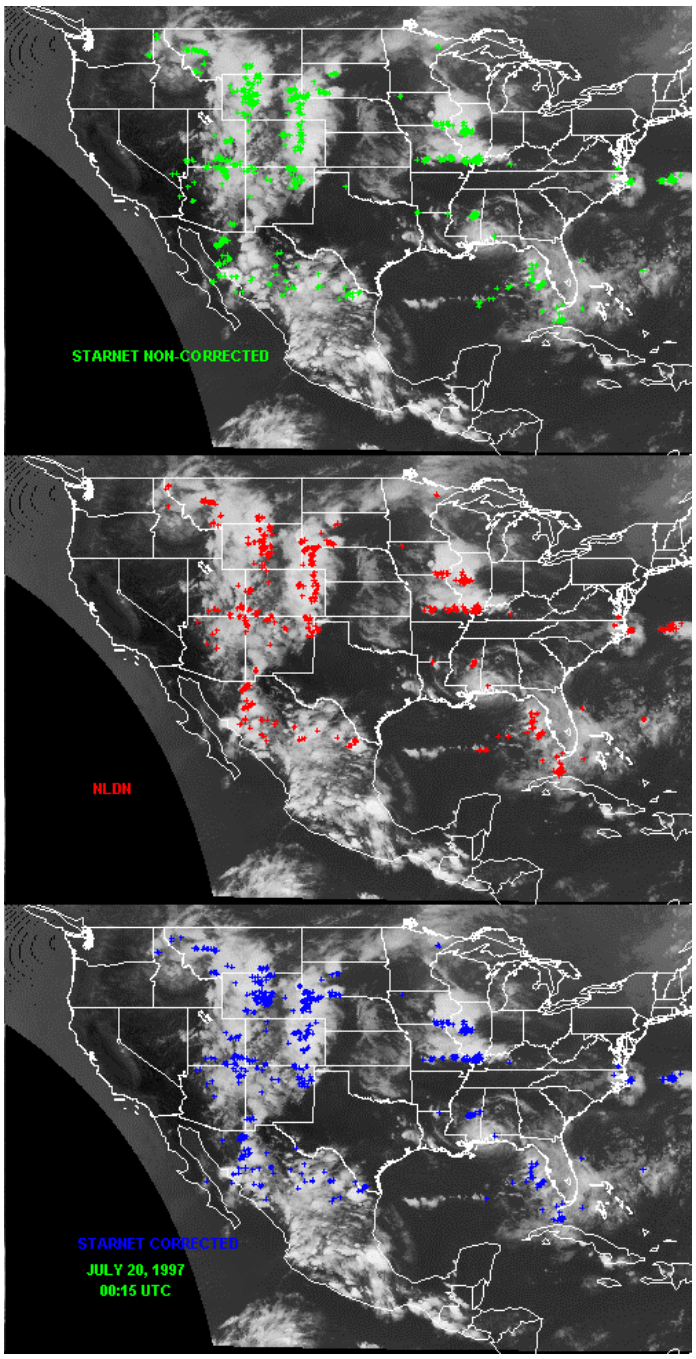

Figure 10. Spatial distribution of lightning as measured by NLDN and STARNET on July 20 1997 at 00:15 UTC superimposed with GOES-8 Infra-Red images. Top panel, shows STARNET without correction. Middle panel shows correspondent NLDN measurements and bottom panel shows STARNET data after location correction is applied.

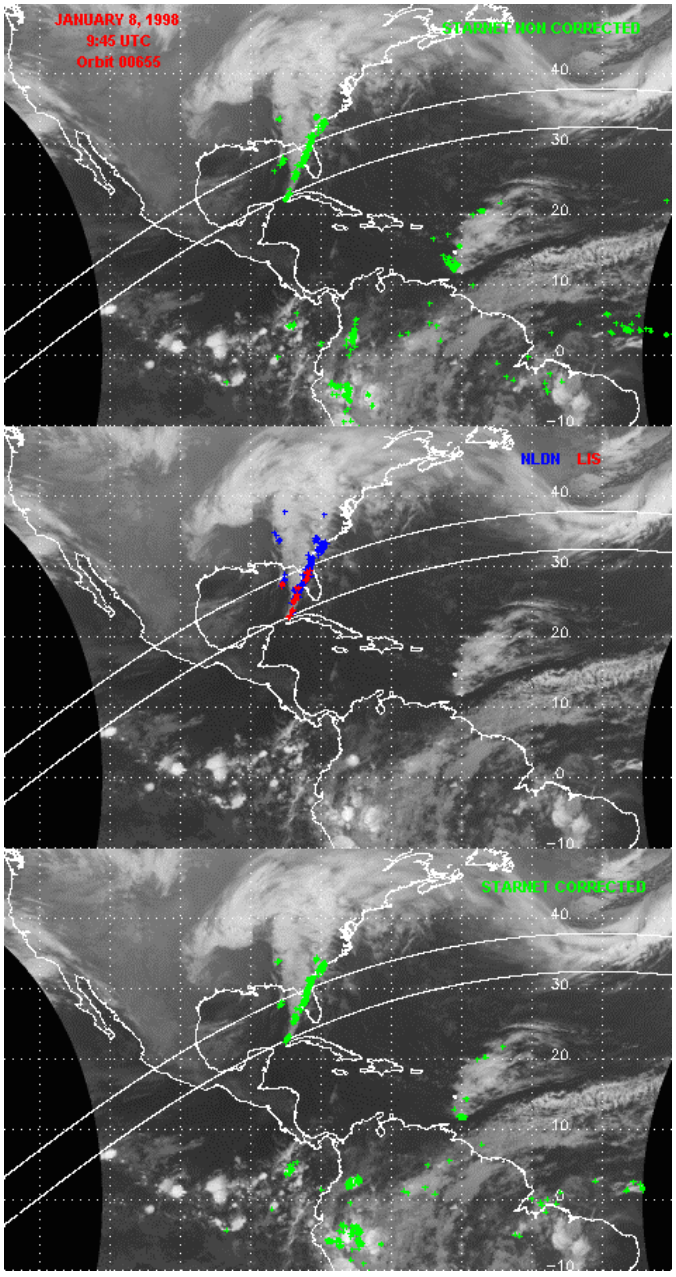

Figure 11. Spatial distribution of lightning as measured by NLDN, LIS and STARNET on January 8 at 09:45 UTC (TRMM orbit 655) UTC superimposed on GOES-8 Infra-Red images. Top panel, shows STARNET without correction. Middle panel shows the corresponding NLDN (blue) and LIS(red) measurements and bottom panel shows STARNET data after location correction is applied.

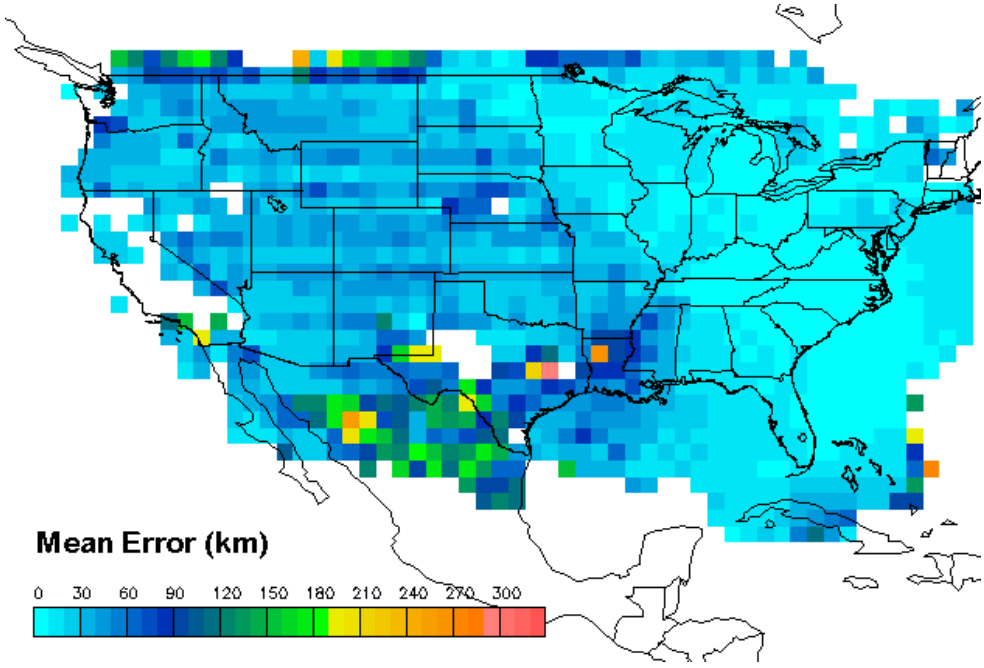

Figure 12. Mean error distribution of STARNET compared to NLDN after the GOES IR image correction is applied.

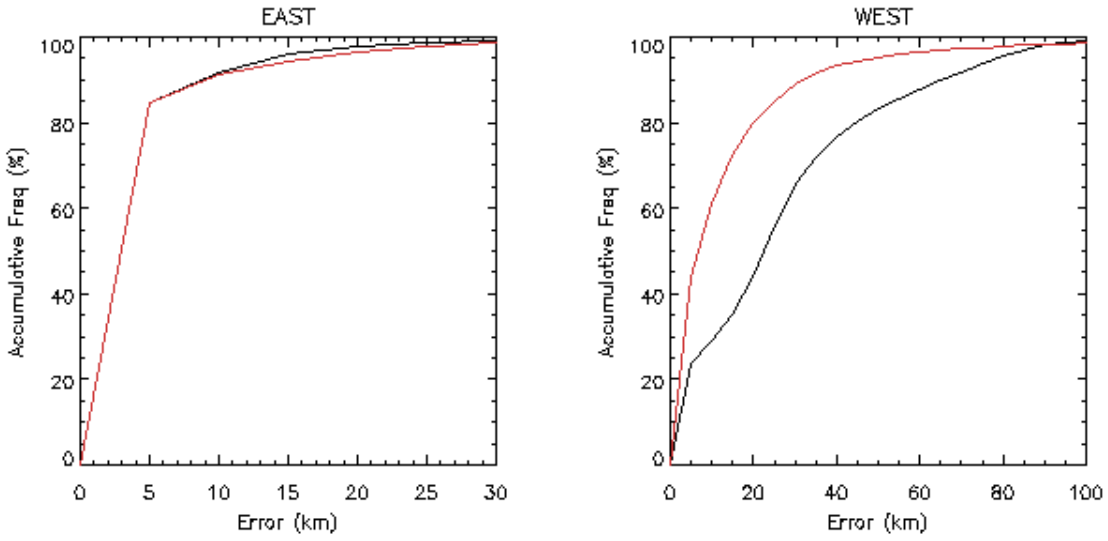

Figure 13. Cumulative error distribution for the (left panel) east coast of US (east of 90W) and (right panel) west coast (west of 90W). The black curve shows the original cumulative distribution and the red line the CDF after the correction is applied.